Applied Spectroscopy Reviews

Hyperspectral Imaging Applications in Agriculture and Agro-Food Product Quality and Safety Control: A Review

Laura M. Dale [a] [b] , André Thewis [a] , Christelle Boudry [a] , Ioan Rotar [b] , Pierre Dardenne [c] , Vincent Baeten [c] & Juan A. Fernández Pierna [c]

[a] Animal Science Unit, Gembloux Agro-Bio Tech, University of Liège, Gembloux, Belgium

[b] Department of Grassland and Forage Crops, University of Agricultural Science and Veterinary Medicine Cluj, Cluj Napoca, Romania

[c] Walloon Agricultural Research Centre, Valorisation of Agricultural Products Department, Gembloux, Belgium
Version of record first published: 03 Jan 2013.

PLEASE SCROLL DOWN FOR ARTICLE

Taylor & Francis
Taylor & Francis Group

Hyperspectral Imaging Applications in Agriculture and Agro-Food Product Quality and Safety Control: A Review

LAURA M. DALE,[1,2] ANDRÉ THEWIS,[1]
CHRISTELLE BOUDRY,[1] IOAN ROTAR,[2]
PIERRE DARDENNE,[3] VINCENT BAETEN,[3]
AND JUAN A. FERNÁNDEZ PIERNA[3]

[1]Animal Science Unit, Gembloux Agro-Bio Tech, University of Liège,
Gembloux, Belgium
[2]Department of Grassland and Forage Crops, University of Agricultural Science
and Veterinary Medicine Cluj, Cluj Napoca, Romania
[3]Walloon Agricultural Research Centre, Valorisation of Agricultural Products
Department, Gembloux, Belgium

Abstract: *In this review, various applications of near-infrared hyperspectral imaging (NIR-HSI) in agriculture and in the quality control of agro-food products are presented. NIR-HSI is an emerging technique that combines classical NIR spectroscopy and imaging techniques in order to simultaneously obtain spectral and spatial information from a field or a sample. The technique is nondestructive, nonpolluting, fast, and relatively inexpensive per analysis. Currently, its applications in agriculture include vegetation mapping, crop disease, stress and yield detection, component identification in plants, and detection of impurities. There is growing interest in HSI for safety and quality assessments of agro-food products. The applications have been classified from the level of satellite images to the macroscopic or molecular level.*

Keywords NIR spectroscopy, satellite system, airborne system, ground-based HSI, NIR-HSI, agriculture, agro-food industry

Introduction

Agricultural materials are characterized by different chemical composition and internal physical structures, which means that, when working with near-infrared (NIR) spectroscopy, they reflect, scatter, absorb, and/or emit electromagnetic energy in different ways at specific wavelengths. These differences are characterized by a typical NIR spectrum that can be considered as the spectral signature or spectral fingerprint of the material. NIR spectroscopy has been a well-known technology in the agricultural sector since the scientific work conducted by Norris and coworkers in the 1960s (1). It is a nondestructive method of analysis based on the diffuse reflectance of samples and is widely used for rapidly determining the

Address correspondence to Laura M. Dale, Animal Science Unit, Gembloux Agro-Bio Tech, University of Liège, 2, Passage des Déportés, 5030 Gembloux, Belgium. E-mail: dale_lm@yahoo.com

concentration of nutrients and feed value in dried and fresh crop materials (2–7), food and feed quality control (8, 9), and food safety (10–12).

In recent years, new methods based on NIR spectroscopy technology have been developed, mainly based on a combination of techniques. Thus, NIR technology has been linked with a microscope to create NIR microscopy (NIRM) (13) and with imaging techniques to create hyperspectral imaging (HSI) methodologies. ElMasry and Sun (14) defined HSI as a "combination of the strong and weak points of visible/near-infrared (VIS/NIR) spectroscopic techniques and vision techniques." The images provide enough information to identify and distinguish spectra as unique material. A hyperspectral image offers the potential to extract more accurate and detailed information than that obtained when working with classical NIR technology. Burger and Geladi (15) noted that NIR-HSI gives us a natural expansion of conventional spectroscopy as well as the spatial position information of the acquired spectra. With the decrease in wavelength resolution, the NIR-HSI spectrum is compensated by increasing the spectral quality obtained from thousands of spectra. NIR-HSI processing algorithms, known as multivariate imaging analysis (MIA), are still being developed. Hyperspectral images have become one of the most common research objectives in the exploration and monitoring technologies used in many areas of work (14).

A NIR spectroscopy system provides one spectrum per measurement, whereas hyperspectral images provide thousands of spectra from one sample. In one measurement, each pixel corresponds to one spectrum. The image taken by NIR-HSI also provides a spectral signature of the sample that is unique and can be used to characterize and identify any given material (16).

The initial uses of these hyperspectral images were for remote sensing applications (detection and mapping) because of the reflection characteristics of the spectra. HSI was used for the detection of military vehicles hidden in vegetation and for some of the National Aeronautics and Space Administration's (NASA) work (17). It was also successfully used by geologists to identify and simultaneously analyze more than 150 materials, including minerals, vegetation, ice, and snow (18). Hyperspectral images give a good enough spectral range and spatial resolution for mapping and studying the Earth's surface and for characterizing soil properties, including moisture, organic matter content, and salinity (19). NIR-HSI is useful in the paper industry for sorting different types of materials (e.g., pulp, paper, cardboard, newspaper, and bleached and unbleached fibers) (20). HSI is very useful in the art domain, not only for artwork conservation (21) but also for identifying pigments in paintings and palimpsests (22).

The technique has been used in the medical sector to determine various diseases, such as peripheral vascular diseases (23), and in ophthalmology and oncology (24), immunohistochemistry (25), latent fingerprinting and age assessment of bruises in forensic medicine (26), and face recognition in biomedicine and human identification (27). Recent studies have demonstrated that HSI can be used in cancer diagnosis (28). The HSI technique is a promising method for evaluating cervical cytologic preparations and, if used in conjunction with slide scanners, can assist in the automated detection of precancerous and cancerous cells. NIR-HSI can be used for mapping compound distribution, testing active pharmaceutical ingredients and excipients for formulation uniformity, identifying contamination on tablet surfaces, and detecting dissolution problems in solid pharmaceutical forms (29, 30).

The objective of this article is to describe HSI and its principles and to compare the advantages and disadvantages of NIR-HSI with the classical NIR spectroscopy technique. The applications described range from landscape to field scale, such as mapping a canopy or highlighting vegetation stress, to the more restricted microscopic, if not molecular, level, such as detecting contaminants or quantifying biochemical parameters.

Principles and Instrumentation

The field of spectral imaging can be divided into three domains: multispectral imaging (MSI), HSI, and ultraspectral imaging (USI). MSI is a system where the image acquired has few separated wavelengths. In HSI, the image is acquired with an abundance of continuous wavelengths. USI is when one image is acquired with a low spatial resolution of several pixels (i.e., the system used has a very fine spectral resolution) (14).

Hyperspectral images or *hypercubes* are three-dimensional data sets containing light intensity measurements where two dimensions (*X* and *Y*) represent spatial positions and the third dimension (λ) represents spectral variation (Figure 1). The images can be interpreted, typically, as stacks of hundreds of two-dimensional spatial images at different wavelengths, or tens of thousands of spectra, aligned in rows and columns.

Three instrumentation approaches are used to acquire hyperspectral images. These approaches can be termed (a) *point* (*staring*) *scan*, (b) *push-broom* (*line*) *scan*, or (c) *plane* (*whiskbroom*) *scan*, depending on the orientation of the scanning dimension relative to the two-dimensional spatial sample axes. A point scan (or staring instrument) acquires a spectrum at a single spatial location using a Fourier transform (FT) or grating-type spectrometer. Hyperspectral images are obtained by successively measuring spectra while the sample is repositioned in the *X* and *Y* spatial dimensions. This kind of instrument is often used in microscopy using a high-precision *X-Y* motion stage. The push-broom system projects a line of light onto a two-dimensional focal plane array (FPA) and is best suited for remote sensing by aircraft or online process measurement because the *Y* spatial axis may be arbitrarily long. The plane scan (or whiskbroom) imaging system positions the measurement camera parallel to the sample surface, obtaining *X-Y* spatial images with fixed sizes limited by the dimensions (pixels) of the camera detector. Hyperspectral images
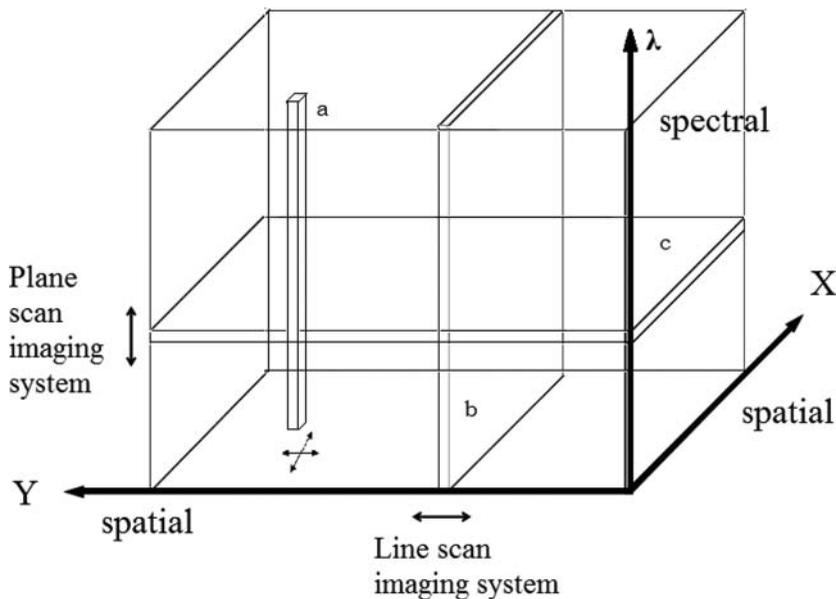

Figure 1. Hyperspectral image (hypercube) aquisitions technique, adapted from Vermeulen et al. (31), (CRA-W) 208 × 145 mm (96 × 96 DPI). Legend: a-scan point (staring) scan, b-push-broom (line) scan, c-plane (global) scan, λ-spectral variation, X and Y-spatial dimensions.
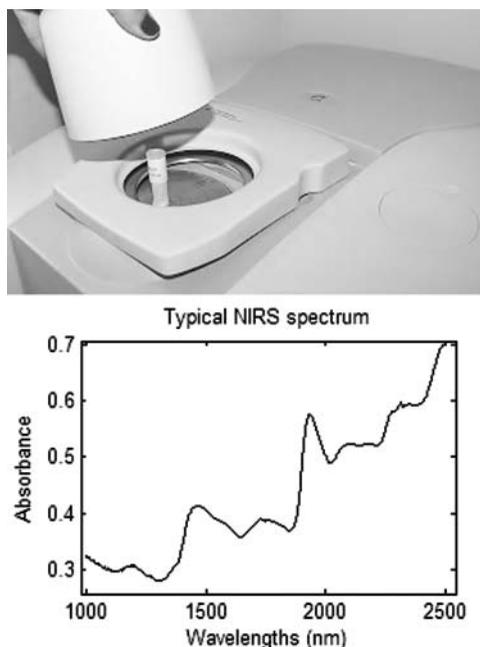
Figure 2. Aquisition of spectrum by conventional NIRS system. Legend: (1) NIRS system; (2) Typical spectrum of NIRS system.

are obtained by modulating the radiation reaching the camera via the use of band-pass or tuneable filters positioned in front of the camera (31–32).

Advantages and Disadvantages of NIR-HSI

For both classical NIR and HSI, the obvious advantages include simplicity of data acquisition, low cost per analysis, rapid inspection, simultaneous analysis of several compounds, nondestructive method, and accuracy. The advantages of all NIR spectroscopy systems are reflected in NIR-HSI systems. In NIR spectroscopy systems, however, the samples usually have to be ground at less than 1 mm, but with NIR-HSI systems sample preparation is not necessary; the samples can be scanned without any grinding and can be used for other purposes (e.g., for germination assays or rescanning when the samples are in different vegetation stages in order to predict the optimal period for harvest) (14).

One of the strong points of NIR-HSI is the time savings, not only for sample preparation but also for database registration (14, 33). With conventional NIR techniques, one measure gives one average spectrum (Figure 2). Thousands of spectra can be obtained with NIR-HSI, giving a complete picture of the distribution of chemical compounds at the pixel level (Figure 3) and the possibility of simultaneously obtaining the spectral and spatial description of the sample (34).

Hyperspectral images can provide high-quality spectra of surfaces (35) related to internal information (e.g., they can detect and quantify bacteria distribution inside the product) (15, 36).

Although this technique has the potential to detect diseases and defects in agricultural products and food, its application is limited due to the price of equipment, a clear
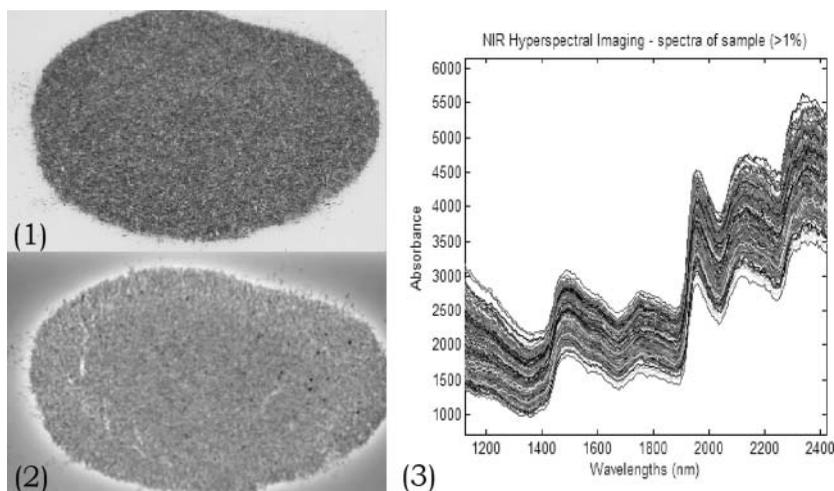
Figure 3. Aquisitions of spectra using a laboratory-scale NIR-HSI system (CRA-W). Legend: (1) Photograph of sample; (2) Hyperspectral image of sample; (3) Typical spectra (<1%) of a laboratory-scale NIR-HSI system.

disadvantage of the method (8). In addition, for rapid image acquisition and analysis, NIR-HSI requires very high hardware speed, a major factor that limits its use (14).

As in the case of NIR spectroscopy, NIR-HSI is an indirect method and calibration models are necessary. This is a disadvantage in both systems. To obtain efficient qualitative and quantitative analyses, NIR spectroscopy and NIR-HIS methods need to be combined with chemometric techniques (29), a discipline that uses mathematical and statistical methods to extract and interpret chemical information from data (37). In the literature there are many reviews and textbooks on chemometrics (29, 37–40). The disadvantage is that all of this modeling and data processing is time consuming; interpretation programs are very expensive and specialists are needed for calibration and standardization.

Another disadvantage of NIR-HIS is the registration of a series of successive overlapping bands; it is difficult to assign them to specific chemical groups and working with what are seen as *bad pixels* (also known as *spies*; Figure 4) (14). In order to identify and detect different unambiguous spectra in the same image, it is necessary for a sample to have the same absorption characteristics (14). López-Alonso and Alda (41) carried out a comprehensive study on bad pixels, defining them as pixels classified as anomalous (e.g., pixels that always produce the same signal and from which chemical information cannot be extracted). Blinking or drifting pixels with erratic behavior can also be called bad pixels, because they are clearly different from those considered good pixels. There are also *noisy pixels* (i.e., pixels emitting a noise higher than a fixed level).

Applications of NIR-HIS Systems

The applications are described here according to the system used, ranging from satellite images to small-scale studies: (1) satellite HSI systems, (2) airborne VIS/NIR systems, (3) ground-based HSI systems, and (4) laboratory-scale HSI systems (Figure 5).
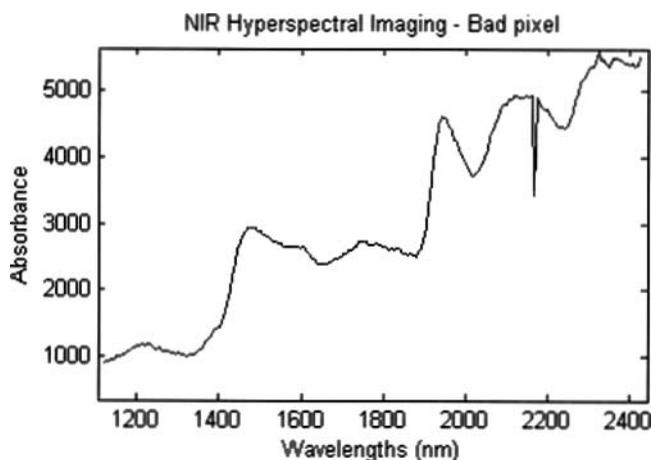
Figure 4. Spectrum of "bad pixel" (spie) (CRA-W).

Satellite HSI Systems

Many studies using satellite systems have been conducted since the 1960s in different domains. The pioneering studies were in the domains of mining and geology (42). In the following years the technique was adapted for agricultural uses, such as determining the physical properties of plant canopies (e.g., leaf size and leaf area index; wavelengths ranged between 400 and 2,400 nm) (43). Many studies focused on the relationship between optical properties and pigment concentration of leaves. For example, Johnson et al. (44) conducted studies on leaf area index and chlorophyll determination and on discrimination between grass, weed, and plastic objects. The focal plane screening used had wavelengths

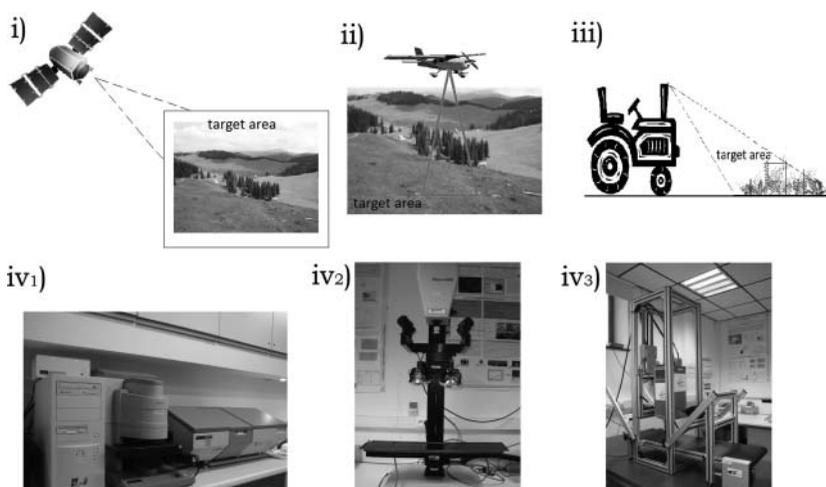**Figure 5.** Hyperspectral Imaging Systems (photo original). (i) Satellite Hyperspectral Imaging Systems; (ii) Airborne Visible/Near Infared Imaging Systems; (iii) Ground-based Hyperspectral Imaging Systems; (iv$_1$) NIR Hyperspectral Imaging Systems-point (staring) scan (CRA-W); (iv$_2$) NIR Hyperspectral Imaging Systems-plane (whiskbroom) scan (CRA-W); (iv$_3$) NIR Hyperspectral Imaging Systems-push-broom (line) scan (CRA-W).

ranging from 330 nm to 1,100 nm, with a 3-nm spectral resolution. Broge and Leblanc (45) investigated the application using satellite data for leaf area index and canopy chlorophyll density under the same methodological conditions (wavelengths 550–1,000 nm). Significant results were produced from monitoring plant growth and estimating the photosynthetic productivity potential.

Other studies have focused on discrimination between plant stresses imposed by limiting water, insufficient nitrogen fertilizer, or both. El-Shikha et al. (46) used a remote sensing monitoring system, the Agricultural Irrigation Imaging System (AgIIs), and showed in 22×22 m plots that the effects of nitrogen treatment were more pronounced on leaf area index, plant canopy width, and fresh yield than the effects of water treatment on broccoli culture. Successful results were obtained at a reflectance band of 720 nm. El-Shikha et al. (46) concluded, however, that it would be better for future studies to use airborne scanning or airborne imagery because it is more practical and less expensive than the satellite systems.

Airborne VIS/NIR Systems

Whereas satellite data focus on canopy studies, airborne hyperspectral data are restricted mainly to terrestrial vegetation (e.g., canopy, leaf area index, plant diseases, plant production, biochemical parameters). In a study on vegetation community stress, Merton (47) used NASA's Airborne Visible/Infrared Imaging Spectrometer (AVIRIS) to map multitemporal trends; these were strongly correlated and were successfully used to predict the biochemical impact and geographical extent of vegetation. Zhang et al. (48) successfully used the same AVIRIS system in combination with spectral angle mapping (SAM) to detect tomato stress induced by late blight disease. The wavelengths ranged from 400 to 2,500 nm, and the spatial resolution was 4 nm. The same technique was used by Parker Williams and Hunt (49) to estimate leafy spurge (*Euphorbia esula* L.) cover in 66 circular vegetation plots with a radius of 23 m (wavelengths 400–2,500 nm; spectral resolution of 10 nm). It is possible to use AVIRIS, however, to estimate leafy spurge distribution and design abundance maps. The differentiation of individual plant species can be problematic because all green plants have similar spectral characteristics.

With a portable hyperspectral tunable imaging system (PHyTIS package), composed of two liquid-crystal tunable filters (Varispec filters, Cambridge Research Instrumentation, Woburn, MA), Fitzgerald (50) successfully identified cotton (*Gossypium hirsutum* L.) fields and estimate cotton production. The absorption was centered on 400–720 nm wavelengths passing from visible light to NIR radiation (650–1,100 nm wavelengths).

Several studies have demonstrated that airborne imaging systems can be successfully used for mapping invasive plants (51, 52). Pengra et al. (51) mapped the common reed (*Phragmites australis* (Cav.) Trin. Ex Steud.) in saltmarsh vegetation (wavelengths 400–2,500 nm). They found spectral differences between *Phragmites* and 26 other saltmarsh vegetation associations at wavelengths below 1,100 nm using SAM and obtained a classification accuracy of 81.40%. Andrew and Ustin (52) used an airborne system (126 wavebands, 3-m spatial resolution, and 450–2,500 nm wavelengths) to map perennial pepperweed (*Lepidium latifolium* L.) on grasslands, using the cellulose absorption index (defined at 2,100 nm). The model used mixture-tuned matched filtering (MTMF), with an accuracy higher than 85%. Fiorani et al. (53) presented a number of selected wavelengths (around 970, 1,600, and 2,100 nm) for specific characteristics of plants, such as chemical composition or canopies.

Ground-Based HSI Systems

With this system, the hyperspectral images are taken at the field level, usually by fixing a camera on an agricultural vehicle. It allows, inter alia, field production to be estimated. Yang et al. (54) estimated grain sorghum yield variability using a CCD camera-based HSI (wavelengths 457–922 nm; 1.5-m spatial resolution). The yield maps generated from the images taken with airborne and ground-based HSI corresponded closely with yield data measured after harvest. Similar results were reported by Schut et al. (55) for grass yield and nutrient content in a field measured at 848–1,680 nm. They reported that the system was very suitable for measuring large fields, especially for ground coverage, index of reflection intensity, and wavelet entropy. Schut et al. (55) reported a consistent correlation between dry matter content estimated with partial least squares (PLS) and ground coverage, index of reflection intensity, and mean reflection at 800 nm.

Using the same approach, Suzuki et al. (56) predicted forage chemical composition (ImSpector V10, Specim, Oulu, Finland; wavelengths 360–1,010 nm; spectral resolution 10 nm). The study was conducted in a field with the aim of mapping the grass chemical components by developing different calibration models; the coefficient of determination for crude protein and total digestible nutrients was higher than 0.70. Okamoto et al. (57) developed a model focusing on weed detection and classification of plants under the same conditions described above. Initially, the plant species were classified and then the plant leaves and background soil were separated. For plant discrimination, the Euclidean distance achieved with segmentation was used, achieving a classification accuracy of 75–80%, whereas discriminant analysis provided an accuracy of 90%. A method for mapping botanical composition and herbage mass in pasture using the same ground-based HSI systems was developed by Suzuki et al. (58). The herbage mass was first measured by linear discriminant analysis (LDA), and the plant species were then classified as perennial ryegrass, white clover, other plants, and dead material, with a classification accuracy of 91.6%.

Laboratory-Scale HSI Systems

Qualitative Applications. One of the first studies using this technology in the agricultural sector focused on the detection of meat and bone meal in compound feedstuffs using HSI in the NIR focal plane MatrixNIR (Malvern Instruments Ltd., Malvern, UK; wavelengths 900–1,700 nm at increments of 6 nm) (59). The method was developed to enforce food legislation adopted after the European mad cow crisis connected with Creutzfeldt-Jakob diseases in humans. Thousands of spectra in a massive space had to be collected simultaneously. For detection, the chemometric support vector machine (SVM) tool was used. This alternative method of NIR focal plane MatrixNIR was suggested as being more effective than methods used at that time, which were cumbersome and required a specialist. Similar studies were carried out by Riccioli et al. (60) for discriminating between terrestrial and fish species in animal protein by-products used in livestock feed. The samples were analyzed by NIR chemical imaging (NIR-CI) in the 1,000–1,700 nm wavelength range. Four algorithms—Mahalanobis distance, Kennard-Stone, spatial interpolation, and binning—were applied in order to select an appropriate subset of pixels for further partial least squares discriminant analysis (PLSDA). For the four algorithms used, the classification accuracy obtained was higher than 99.61%.

Kim et al. (61) used fluorescence HSI for the detection of skin tumors (ulcerous lesions surrounded by a rim of thickened skin and dermis) on chicken carcasses, replacing the time-consuming, expensive, and uncomfortable organoleptic inspection method. They

used an HSI system from the U.S. Department of Agriculture's Instrumentation and Sensing Lab (ISL-HSI), which includes a CCD camera, a spectrograph, a sample transport mechanism, and lighting sources (wavelengths 425–711 nm). The detection rate was 76%, indicating that the method needs to be improved; some spots were irrelevant for tumors and some carcasses were not filtered out in the spatial classifier, giving a false-positive rate that was too high. Various studies were conducted to detect the contamination of poultry carcasses with visceral content (62, 63). In order to demonstrate that it is possible to detect fecal and ingested contaminants using NIR-HSI, Lawrence et al. (62) and Park et al. (63) used an imaging camera consisting of a focusing lens, a prism-grating spectrograph, and a high-resolution CCD camera. Park et al. (63) used the region of interest (ROI) algorithm at wavelengths of 290–1,000 nm and obtained an accuracy of 96.6% using principal component analysis (PCA). The imaging system operated from wavelengths of about 400 to 900 nm (62). Similar studies were carried out by Wang and El Masry (64) for apple bruise detection based on physical and chemical changes compared with unbruised fruits (wavelengths 400–1,000 nm). They developed a model using different algorithms: minimum noise fraction transform (MNF), ROI, PCA, PLS, and artificial neural networks (ANNs). The 750-, 820-, and 960-nm wavelengths were chosen for bruise detection. In order to determine the potential of the selected wavelengths for bruise detection, PCA was conducted with successful results, such as 93.25% of the variance between normal and bruised spectral data (principal component 1 [PC1]: 70.01% and principal component 2 [PC2]: 23.94%). Nagata et al. (65) and Nagata and Tallada (66) worked successfully on strawberry bruise detection. The LDA algorithm was used at a range of 825 and 980 nm and the rate of discrimination was greater than 90.70% for the calibration model, whereas for validation it was greater than 86.50%. Other applications of the ISL-HSI system were used for vegetables. The system was used successfully for detecting cucumber chilling injury, with recognition rates of 93.30% for injured cucumbers and 88.30% for uninjured cucumbers (67). With this system, the hyperspectral images were acquired at wavelengths of 448–951 nm, with a 4.5-nm interval. For detection, PCA and Fisher's linear discrimination (FLD) were used.

NIR-HSI is also used to measure food quality, particularly fruit quality. For consumer acceptance and fruit shelf life, firmness is very important and it is necessary for the industry to use a nondestructive sensing system to evaluate it. High scattering from a surface depends on the cell structure of the food and is related to the texture. Scattering profiles can therefore be used to predict fruit firmness. A VIS/NIR-HSI system based on a Varispec Liquid Crystal Tunable Filter (LCTF, Cambridge Research and Instrumentation) was used for firmness detection, and LDA, normalized difference (ND), and ANN algorithms were used to analyze the spectra (66). For strawberry firmness detection, wavelengths of 665–685, 755–870, and 955–1,000 nm were shown to be optimal (standard error of prediction [SEP] around 0.258 in the case of 70% to fully ripe strawberries and 0.350 in the case of 50% to fully ripe strawberries) (66). A similar technique was used by Lu and Peng (68) to determine peach firmness. The most important bands for predicting peach firmness were found to be around 677, 710–850, and 950 nm. The Lorentzian distribution (LD) parameter combinations for firmness calibration of two types of peaches (Red Haven and Coral Star) were chosen. The coefficients of determination (R^2) obtained with multilinear regression (MLR) were between 0.51 and 0.58 and between 0.67 and 0.77, respectively. In both cases, further analysis was needed to obtain better results.

Beef color and tenderness are two major parameters of beef quality. Beef quality evaluation by a trained panel is expensive, time consuming, and difficult to organize. The development of a nondestructive, fast, accurate, on-line technology for predicting beef color and tenderness is therefore highly desirable. As noted above for fruit firmness, hyperspectral

scattering profiles would be useful for assessing beef quality because light scattering from a surface is closely related to product texture. Recently, a VIS/NIR-HSI (400–1,100 nm) was used to predict the beef color parameters and tenderness (Warner-Bratzler shear force) of Luxi cattle between 25 and 36 months old, at carcass weights of 280–450 kg (69). These authors fitted scattering profiles derived from hyperspectral images to the LD function in order to extract parameters that were used to predict the tenderness and color of 7-day-old cooked beef steaks. The LD function parameter contributions of optimal wavelengths were used to establish MLR models. The R^2 for calibration and cross-validation was higher than 0.91 and the overall accuracy of classification in tender and tough groups was 93.8%. Using a push-broom HSI with a diffuse flood lighting system, Naganathan et al. (70) classified beef tenderness into categories (tender, intermediate, and tough) with a classification accuracy of 96.4%, and Kim et al. (71), using an optical scattering feature of lights, obtained an accuracy of 98.4%, although they did not provide details about the type of beef, age, or genotypes of the animals and the carcass weights. These results highlight the potential of HSI optical scattering for the on-line detection of beef quality.

Other studies on contaminant determination have been conducted by Gómez-Sanchis et al. (40) on citrus fruits to detect *Penicillium* fungi. They used a hyperspectral vision system based on liquid-crystal tunable filters (LCTF; Xenoplan, Schneider Optics, Coalsnap ES model, Photometrics), with ranges between 400 and 720 nm for VIS spectral wavelengths and between 650 and 1,100 nm for NIR spectral wavelengths. The aim of the study was to prevent or at least reduce associated economic losses in citrus culture. The accuracy of the classifying methods such as ANN and decision trees was about 98%. The same technique, but with LDA and classification and regression tree models (CART), was used for mandarin fruit and the classification accuracy of rotten fruit was greater than 91% (72).

Another application of HSI in the field of fruit diseases is the detection of citrus canker. Caused by a bacteria, *Xanthomonas axonopodis* Hasse, this is a severe and devastating disease that can affect the peel (conspicuous and erumpent lesions) of some citrus varieties in infected regions of the world. Currently, there is no really effective treatment or prevention to eradicate the disease. The spectral information and divergence (SID) algorithm was recommended by Chang (38) to classify the fruits. It is based on a stochastic approach called *spectral information measure*, which has been shown to outperform classical spectral matching techniques. In this application, SID is interesting for differentiating canker disease from normal and other common diseased peel lesions (73). The HSI wavelengths ranged from 450 to 930 nm and the overall classification accuracy for grapefruit was 96.2%, using an optimal SID threshold value of 0.008 based on the assumption that the false-negative and false-positive errors were equally weighted. The method could therefore be used to discriminate citrus canker from other peel diseases, but more research is needed to improve detection accuracy and make it suitable for online application.

NIR-HSI was used by Fernández Pierna et al. (37) to screen compound feeds. A model was constructed by sorting the particles, using a classification tree where every node encountered a discriminating step. These measures were complemented by discriminating equations created from hyperspectral databases for each class of materials obtained in the MatrixNIR (wavelength range 900–1,700 nm). Discriminating equations were constructed using chemometric SVM tools and classification accuracy was greater than 99% for calibration data and greater than 88% for validation data. Later, Fernández Pierna et al. (74) carried out a similar study on impurity discrimination (straw, broken grains, grains from other crops, weed seeds, insects, plastic, stones, pieces of wood and paintings, animal feces) in cereals (wheat, spelt, and barley). SVM was used as a chemometric tool and classified the impurities with an accuracy of more than 95%.

Burger and Geladi (15) used MatrixNIR at wavelengths of 960–1,662 nm and different algorithms (PLS, ROI, and PCA) to successfully discriminate different types of cheeses on the basis of the protein, fat, and carbohydrate content. The same technique was used to discriminate salt and sugar granules by the peaks centred at 1,130, 1,438, and 1,470 nm, which correspond to salicylic acid, sugar, and citric acid, respectively. Abdel-Nour and Ngadi (75) used HSI to detect omega-3 fatty acids in designer eggs. ROI was used to select the specific spectral region (994 and 1,109 nm), and for discriminant analysis the *K*-means algorithm was used, with 100% accuracy. For egg classification, the PLS algorithm was used. The R^2 coefficients were 0.89, 0.54, and 0.75 and the residual predictive deviations (RPDs) were 2.85, 1.30, and 2.00, respectively, for linolenic acid, eicosapentaenoic acid, and docosahexaenoic acid, respectively.

Quantitative Applications. Peirs et al. (76, 77) and Menesatti et al. (78) applied the hyperspectral technique to determine the starch index of apples as a maturity parameter for predicting the optimal harvest period. They used NIR-HSI equipped with a scanner and spectrophotometer at wavelengths of 1,000–1,700 nm. The PLSDA algorithm was used with a correlation coefficient higher than 0.94. Weinstock et al. (79) used the same technique to predict oil and oleic acid concentration in individual corn kernels. The germ from the endosperm was first distinguished by the PCA algorithm, and then the PLS algorithm was used to successfully predict the total oil and oleic acid concentration, with a root mean standard error of prediction (RMSEP) of 0.7 and 14%, respectively. Alpha-amylase activity was also predicted in Canadian western red spring wheat samples; the analyses were performed by FT-NIR and short-wavelength infrared HSI (SWIR-HSI); the wavelength range was 1,235–2,450 nm and the PCA and PLS algorithms were used (80, 81). A spectral information divergence was registered at a wavelength of 1,900 nm, where water, starch, and protein were believed to be the combination vibrations of overtones of alpha-amylase activity (10, 81, 82). It was pointed out that models built with both systems were similar; the R^2 for FT-NIR was lower than for SWIR-HSI (0.82 and 0.88, respectively) and the root mean square error was 0.90 for FT-NIR and 0.52 for SWIR-HSI.

A MatrixNIR camera and a SisuChema SWIR-HSI system (Specim, Spectral Imaging Ltd., Oulu, Finland) were used to differentiate glassy from floury maize endosperm (wavelengths 960–1,662 nm for the MatrixNIR camera and 1,000–2,498 nm for the SWIR-HSI) (83). The results showed the ability of the PLSDA model to predict glassiness and flouriness correctly with a RMSEP of 0.294. Bauriegel et al. (84) used HSI (wavelengths 400–1,000 nm, spectral resolution 2.5 nm) for the early detection of *Fusarium* infection in wheat. During the development stages, the healthy and diseased tissues could successfully be distinguished with 87% accuracy and were in a ±10% range of tolerance. Similarly, Firrao et al. (85) used the HSI technique for maize fumonisin detection. Because mycotoxins are known to be difficult to detect directly using optical methods, the aim of the study was to scan the contaminated samples at wavelengths from 720 to 940 nm. The authors considered that HSI could provide a reliable contamination estimation (SEP was 0.1895) within a few minutes and be used to assist in lot selection at various stages of the maize processing chain.

Del Fiore et al. (86) built a model of discrimination for healthy and diseased maize kernels produced by toxic fungi with HSI (ImSpector Specim V10, Borgo Isonzo, LT, Italy). The VIS/NIR range was 400–1,000 nm. Using PCA, toxic fungi in maize kernels at specific wavelengths (410, 535, and 945 nm) were detected. In cereals, Vermeulen et al. (87) used MatrixNIR (wavelengths range 900–1,700) to discriminate the ergot bodies from

wheat kernels. The Fisher coefficient calculated on the preprocessed data (wavelength range 1,220–1,440 nm) allowed contaminated samples to be detected.

Plant diseases remain the major problem in crop production, leading to yield and quality loss (88). An NIR line scan or push-broom imaging spectrometer (Burgermetrics, SIA, Riga, Latvia), which uses a cooled, temperature-stabilized mercury–cadmium–telluride detector (Xenics SPECIM Ltd., Oulu, Finland) combined with a conveyor belt (wavelength range 1,100–2,400 nm), was used to quantify crop parameters, such as beet cyst nematodes (*Heterodera schachtii* A. Schmidt) (74, 89). The specific pixels corresponding to the conveyor belt showed higher absorbance around wavelengths of 1,690 and 1,970 nm; the chemometrics tool used in both studies was SVM.

HSI has been used successfully in food and water bacterial contamination detection (39). Some fresh vegetables are common vehicles for foodborne pathogens (e.g., *Salmonella* ssp., *Escherichia coli* O157:H7, *Listeria monocytogenes*). NIR spectroscopy has been used for the analysis of microorganisms in vegetables but does not provide information on bacteria distribution on the product. Siripatrawan et al. (36) have developed an HSI method for the detection of *E. coli* K12 in packaged fresh spinach with minimal human interference. They used a hyperspectral camera with a wavelength range of 400–1,000 nm and a spectral resolution of 5 nm to acquire hyperspectral images. Chemometrics, including PCA and ANN, were then used to analyze the preprocessed data. The predicted number of *E. coli* vs. true values was closely fitted ($R^2 = 0.97$) and the prediction mean square error was very low (MSE = 0.038).

Conclusions and Future Developments in HSI

In this review, a wide range of HSI applications in agriculture and agro-food quality and safety, from a macroscopic approach to a more limited field area, has been described.

Among the various HSI systems, satellite and airborne HSI shows a weakness in the conformity between the information acquired through interpretation of the images and the data acquired in the field, leading to possible errors. With ground-based HSI, it is simpler to determine whether the data are similar or not, but errors are still possible because not only are the samples registered but the background can be intercepted also, and it is necessary to improve the technique to obtain lower prediction errors. Finally, with NIR-HSI, errors are not registered on a large scale because data are collected directly on samples, on sample surfaces, or from the inside of samples for specific component detection or discrimination. However many errors have been registered, such as sampling, pixel overlapping, penetration depth, lack of fit, etc.

Compared with classical analytical methods (e.g., high-performance liquid chromatography, mass spectroscopy), as a nondestructive, fast, nonpolluting, and relatively low-cost method, HSI is an emerging technology for diversified applications in agriculture and in food quality and safety. Its ability to determine the internal constituents of food products is of prime importance in the food industry. In addition, compared with the other imaging systems, NIR-HSI is able to provide spatial and spectral information as well as multiconstituent information, and it is sensitive to minor constituents. But if the analyte of interest is concentrated in spots and if it is homogeneously distributed, the limit of detection will be determinated as with conventional NIR.

There is growing interest in using HSI in agriculture and the agro-food industry to control and predict agro-food quality through specific components analyses but also for the on-line detection of diseases and chemical, microbial, or biological contaminants.

This article has shown that HSI can be used successfully in grassland studies on a large scale, but the system is not yet developed enough for species discrimination on dried and milled samples. HSI could be used for the discrimination of botanical families and plant species and for the detection of toxic and invasive plants from mixed meadows.

With regard to future developments other than applications in agriculture and food quality and safety, it is necessary to develop low-cost HSI systems for dedicated applications (e.g., by identifying optimal wavelengths/wavebands depending on the application for which it is intended). An improvement in preprocessing speed and robustness, particularly in the reliability of models, could encourage more widespread online utilization of this technology in agriculture and the agro-food industry, which could therefore reduce the cost of process monitoring and product inspection.

Acknowledgments

List of Abbreviations

HPLC: High Performance Liquid Chromatography
MS: Mass Spectroscopy
IR: Infrared Spectroscopy
NIRS: Near Infrared Spectroscopy
HSI: Hyperspectral Imaging
MSI: Multispectral Imaging
USI: Ultraspectral Imaging
FT-NIR: Fourier Transform Near Infrared
IR-HSI: Infrared Hyperspectral Imaging Spectroscopy
NIR-HSI: Near Infrared Hyperspectral Imaging System
VIS: Visible
FPA: Focal Plane Array
AVIRIS: Airborne Visible/Infrared Imaging Spectrometer
SWIR-HSI: Short Wavelength Infrared Hyperspectral Imaging System
ISL-HSI: Instrumentation and Sensing Lab Hyperspectral Imaging System
PHyTIS: Portable Hyperspectral Tunable Imaging System
PCA: Principal Component Analysis
PCR: Principal Component Regression
MLR: Multi-Linear Regression
PLS: Partial Least Squares Regression
PLSDA: Partial Least Squares Discriminant Analysis
LDA: Linear Discriminant Analysis
SVM: Support Vector Machines
ANN: Artificial Neural Networks
SID: Spectral Information and Divergence
LD: Lorentzian Distribution
SEC: Standard Error of Calibration
SECV: Standard Error of Cross-Validation

SEP: Standard Error of Prediction
RPD: Residual Predictive Deviation
WBSF: Warner Bratzler Shear Force

References

1. Hart, J., Norris, K., and Golumbie, C. (1962) Determination of the moisture content of seeds by near-infrared spectroscopy. *Cereal Chem.*, 39: 94–99.
2. Murray, I. (1986) Near infrared reflectance analysis in forages. In *Recent Advances in Animal Nutrition*, Haresign, W. and Cole, D.J., Eds. Butterworth: London, pp. 141–156.
3. Biston, R., Dardenne, P., and Demarquilly, C. (1989) Determination of forage in vivo digestibility by NIRS. In Desroches, R., ed. Proceedings of the XVI International Grassland Congress, Association Française pour la Production Fourragere Versailles: Nice, France, 4–11 October, 1989, pp. 895–896.
4. Dardenne, P., Agneessens, R., and Biston, R. (1992) La spectrométrie dans le proche infrarouge, outil analytique de gestion de la qualite des produits agricoles et de l'environnement. *Bull. des Rech. Agron. Gembloux*, 27: 39–51.
5. Vidican, R.M., Rotar, I., and Sima, N.F. (2000) Tehnica NIRS (near infrared reflectance spectroscopy) şi aplicaţiile sale în analiza calităţii furajelor. *Simpo. Agricultura şi Alimentaţia*, USAMV Cluj, Romania: 187–191.
6. Decruyenaere, V., Lecomte, P., Demarquilly, C., Aufrere, J., Dardenne, P., Stilmant, D., and Buldgen, A. (2009) Evaluation of green forage intake and digestibility in ruminants using near infrared reflectance spectroscopy (NIRS): Developing a global calibration. *Animal Feed Science and Technology*, 148 (2–4): 138–156.
7. Rotar, I., Dale, L.M., Vidican, R.M., Mogos, A., and Ceclan, O.A. (2009). Research on protein content and toral nitrogen of maize cob and strains by FT-NIR spectrometry. *Bull. UASVM Cluj*, 66 (1): 465–467.
8. Chen, Y.R., Chao, K., and Kim, M.S. (2002) Machine vision technology for agricultural applications. *Comput. Electron. Agr.*, 36: 173–191.
9. Salguero-Chaparro, L., Baeten, V., Abbas, O., and Peña-Rodríguez, F. (2012) On-line analysis of intact olive fruits by VIS-NIR spectroscopy: Optimisation of the acquisition parameters, *J. Food Eng*, 112 (3): 152–157. doi: 10.1016/j.jfoodeng.2012.03.034
10. Fernández-Ibanez, V., Soldado, A., Martinez-Fernández, A., and de la Roza-Delgado, B. (2009) Application of near infrared spectroscopy for rapid detection of aflatoxin B1 in maize and barley as analytical quality assessment. *Food Chem.*, 113: 629–634.
11. Santos, C., Fraga, M.E., Kozakiewicz, Z., and Lima, N. (2010) Fourier transform infrared as a powerful technique for the identification and characterization of filamentous fungi and yeasts. *Res. Microbiol.*, 161: 168–175.
12. Pei, X., Tandon, A., Alldrick, A., Giorgi, L., Huang, W., and Yang, R. (2011) The China melamine milk scandal and its implications for food safety regulation. *Food Pol.*, 36: 412–420.
13. Yang, Z., Hana, L., Fernández Pierna, J.A., Dardenne, P., and Baeten, V. (2011) Review: The potential of near infrared microscopy to detect, identify and quantify processed animal by-products. *J. Near Infrared Spectros.*, 19 (4): 211–231.
14. ElMasry, G. and Sun, D.W. (2010) Principles of hyperspectral imaging technology. In *Hyperspectral Imaging for Food Quality Analysis and Control*, Sun, D.-W., ed. Academic Press: San Diego, pp. 3–43.
15. Burger, J. and Geladi, P. (2006) Hyperspectral NIR imaging for calibration and prediction: A comparison between image and spectrometer data for studying organic and biological samples. *Analyst*, 131: 1152–1160.
16. Shaw, G. and Manolakis, D. (2002) Signal processing for hyperspectral image exploitation. *IEEE Signal Process. Mag.*, 19 (1): 12–16.
17. Shippert, P. (2003) Introduction to hyperspectral image analysis. *Space Comm.*, 3: p. 13.

18. Clark, R.N. and Swayze, G.A. (1995) Mapping minerals, amorphous materials, environmental materials, vegetation, water, ice and snow, and other materials: The USGS tricorder algorithm. Paper presented at the Fifth Annual JPL Airborne Earth Science Workshop, In Green, R.O., ed. Summaries of the Fifth Annual JPL Airborne Earth Science Workshop, Pasadena, CA, USA, 23–26 January, JPL Publication, 95(1): 39–40.

19. Ben-Dor, E., Patin, K., Banin, A., and Karnieli, A. (2002) Mapping of several soil properties using DAIS-7915 hyperspectral scanner data. A case study over clayey soils in Israel. *Int. J. Rem. Sens.*, 23 (6): 1043–1062.

20. Tatzer, P., Wolf, M., and Panner, T. (2005) Industrial application for inline material sorting using hyperspectral imaging in the NIR range. *R. Time Imag.*, 11: 99–107.

21. Fischer, C. and Kakoulli, I. (2006) Multispectral and hyperspectral imaging technologies in conservation: Current research and potential applications. *Rev. Conservat.*, 7: 3–16.

22. Rapantzikos, K. and Balas, C. (2005) Hyperspectral imaging: Potential in non-destructive analysis of palimpsests. IEEE ICIP 2005, Genova, Italy, 11–14 September 2005, 2: 618–621.

23. Kellicut, D.C., Weiswasser, J.M., Arora, S., Freeman, J.E., Lew, R.A., Shuman, C., Mansfield, J.R., and Sidawy, A.N. (2004) Emerging technology: Hyperspectral imaging. *Perspect. Vasc. Surg.*, 16: 53–57.

24. Harvey, A.R., Lawlor, J., McNaught, A.I., and Fletcher-Holmes, D.W. (2002) Hyperspectral imaging for the detection of retinal disease. *Proc. SPIE*, 4816: 325–335.

25. Levenson, R.M., Wachman, E.S., Niu, W., and Farkas, D.L. (1998) Spectral imaging in biomedicine: A selective overview. *Proc. SPIE*, 3438: 300–312.

26. Bartick, E.G., Schwartz-Perlman, R., Bhargava, R., Schaeberle, M., Fernandez, D., and Levin, I. (2002) Spectrochemical analysis and hyperspectral imaging of latent fingerprints. Paper presented at the 16th IAFS Meeting, Montpellier, France, 2–7 September 2002, Monduzzi Editore, Bologne, Italy: 61–64.

27. Pan, Z., Healey, G., Prasad, M., and Tromberg, B. (2003) Face recognition in hyperspectral images. *IEEE Trans. Pattern Anal. Mach. Intell.*, 25 (12): 1552–1560.

28. Siddiqi, A.M., Li, H., Faruque, F., Williams, W., Lai, K., Hughson, M., Bigler, S., Beach, J., and Johnson, W. (2008) Use of hyperspectral imaging to distinguish normal, precancerous, and cancerous cells. *Cancer*, 114: 13–21.

29. Roggo, Y., Edmond, A., Chalus, P., and Ulmschneider, M. (2005) Infrared hyperspectral imaging for qualitative analysis of pharmaceutical solid forms. *Anal. Chim. Acta*, 535: 79–87.

30. Gendrin, C., Roggo, Y., and Collet, C., (2007) Content uniformity of pharmaceutical solid dosage forms by near infrared hyperspectral imaging: A feasibility study. *Talanta*, 73 (4): 733–741.

31. Vermeulen, P., Fernández Pierna, J.A., Burger, J., Tossens, A., Dardenne, P., and Baeten, V. (2010) NIR hyperspectral imaging and chemometrics as a lab tool for the quality control of agricultural products. Poster session presented at Chemometrics and Analytical Chemistry (CAC 2010), Antwerp, Belgium, 18–21 October, 2010.

32. Fernández Pierna, J.A., Baeten, V., Dubois, J., Burger, J., Lewis, E.N., and Dardenne, P. (2009) NIR imaging—Theory and applications. In *Comprehensive Chemometrics*, Vol. 4, Brown, S., Tauler, R., and Walczak, B., Eds. Elsevier: Oxford, pp. 173–196.

33. Vigneau, N., Ecarnot, M., Rabatel, G., and Roumet, P. (2011) Potential of field hyperspectral imaging as a nondestructive method to assess leaf nitrogen content in wheat. *Field Crop. Res.*, 122: 25–31.

34. Piqueras, S., Burger, J., Tauler, R., and de Juan, A. (2012) Relevant aspects of quantification and sample heterogeneity in hyperspectral image resolution. *Chemometr. Intell. Lab. Syst.*, 117: 169–182.

35. Amigo, J.M., Cruz, J., Bautista, M., Maspoch, S., Coello, J., and Blanco, M. (2008) Study of pharmaceutical samples by NIR chemical image and multivariate analysis. *Trends Anal. Chem.*, 27 (8): 696–713.

36. Siripatrawan, U., Makino, Y., Kawagoe, Y., and Oshita, S. (2011) Rapid detection of *Escherichia coli* contamination in packaged fresh spinach using hyperspectral imaging. *Talanta*, 85: 276–281.

37. Fernández Pierna, J.A., Baeten, V., and Dardenne, P. (2006) Screening of compound forages using NIR hyperspectral data. *Chemometr. Intell. Lab. Syst.*, 84: 114–118.

38. Chang, C.I. (2000) An information theoretic-based approach to spectral variability, similarity and discriminability for hyperspectral image analysis. *IEEE Trans. Inform. Theory*, 46 (5): 1927–1932.

39. Gowen, A.A., O'Donnell, C.P., Cullen, P.J., Downey, G., and Frias, J.M. (2007) Hyperspectral imaging—An emerging process analytical tool for food quality and safety control. *Trends Food Sci. Tech.*, 18: 590–598.

40. Gómez-Sanchis, J., Martín-Guerrero, J.D., Soria-Olivas, E., Martínez-Sober, M., Magdalena-Benedito, R., and Blasco, J. (2012) Detecting rottenness caused by *Penicillium* genus fungi in citrus fruits using machine learning techniques. *Expert Syst. Appl.*, 39: 780–785.

41. López-Alonso, J.M. and Alda, J. (2002) Bad pixel identification by means of principal components analysis. *Opt. Eng.*, 41: 2152–2157.

42. van der Meer, F.D., van der Werff, H.M.A., van Ruitenbeek, F.J.A., Hecker, C.A., Bakker, W.H., Noomen, M.F., van der Meijde, M., Carranza, E.J.M., Boudewijn de Smeth, J., and Woldai, T. (2012) Multi- and hyperspectral geologic remote sensing: A review. *International Journal of Applied Earth Observation and Geoinformation*, 14 (1): 112–128.

43. Landgrebe, D. (2002) Hyperspectral Image data analysis. *IEEE Signal Process. Mag.*, 19: 17–28.

44. Johnson, B., Joseph, R., Nischan, M., Newbury, A., Kerekes, J., Barclay, H., Willard, B., and Zayhowski, J. (1999) A compact, active hyperspectral imaging system for the detection of concealed targets. *Proc. SPIE*, 3710: 144–153.

45. Broge, N.H. and Leblanc, E. (2001) Comparing prediction power and stability of broadband and hyperspectral vegetation indices for estimation of green leaf area index and canopy chlorophyll density. *Rem. Sens. Environ.* 76 (2000): 156–172.

46. El-Shikha, D., Waller, P., Hunsaker, D., Clarke, T., and Barnes, E. (2007) Ground-based remote sensing for assessing water and nitrogen status of broccoli. *Agr. Water Manag.*, 92 (3): 183–193.

47. Merton, R.N. (1999) Multi-temporal analysis of community scale vegetation stress with imaging spectroscopy. Doctoral Thesis, Department of Geography, University of Auckland, New Zealand.

48. Zhang, M., Qin, Z., Liu, X., and Ustin, S.L. (2003) Detection of stress in tomatoes induced by late blight disease in California, USA, using hyperspectral remote sensing. *International Journal of Applied Earth Observation and Geoinformation*, 4: 295–310.

49. Parker Williams, A. and Hunt, E.R., Jr. (2002) Estimation of leafy spurge cover from hyperspectral imagery using mixture tuned matched filtering. *Rem. Sens. Environ.* 82 (2–3): 446–456.

50. Fitzgerald, J.G. (2004) Notes and unique phenomena precision agriculture. Portable hyperspectral tunable imaging system (PHyTIS) for precision agriculture. *Agron. J.*, 96: 311–315.

51. Pengra, B.W., Johnston, C.A., and Loveland, T.R. (2007) Mapping an invasive plant, *Phragmites australis*, in coastal wetlands using the EO-1 Hyperion hyperspectral sensor. *Rem. Sens. Environ.*, 108: 74–81.

52. Andrew, M.E. and Ustin, S.L. (2008) The role of environmental context in mapping invasive plants with hyperspectral image data. *Rem. Sens. Environ.*, 112 (12): 4301–4317.

53. Fiorani, F., Rascher, U., Jahnke, S., and Schurr, U. (2011) Imaging plants dynamics in heterogenic environments. *Curr. Opin. Biotechnol.*, 23: 1–9.

54. Yang, C., Everitt, J.H., and Davis, M.R. (2003) A CCD Camera-based hyperspectral imaging system for stationary and airborne applications. *Geocarto International*, 18 (2): 71–80.

55. Schut, A.G.T., Van Der Heijden, A.M., Hoving, I., Stienezen, M.W., Van Evert, F.K., and Meuleman, J. (2006) Imaging spectroscopy for on-farm measurement of grassland yield and quality. *Agron. J.*, 98: 1318–1325.

56. Suzuki, Y., Okamoto, H., Takahashi, M., Kataoka, T., and Shibata, Y. (2012) Mapping the spatial distribution of botanical composition and herbage mass in pastures using hyperspectral imaging. *Grassland Science*, 58 (1): 1–7.

57. Okamoto, H., Murata, T., Kataoka, T., and Hata, S.I. (2007) Plant classification for weed detection using hyperspectral imaging with wavelet analysis. *Weed Biol. Manag.*, 7 (1): 31–37.

58. Suzuki, Y., Tanaka, K., Kato, W., Okamoto, H., Kataoka, T., Shimada, H., Sugiura, T., and Shima, E. (2008) Field mapping of chemical composition of forage using hyperspectral imaging in a grass meadow. *Grassland Science*, 54 (4): 179–188.

59. Fernández Pierna, J.A., Michotte Renier, A., Baeten, V., and Dardenne, P. (2004) IR camera and chemometrics (SVM): The winner combination for the detection of MBM. Paper presented at the Stratfeed Symposium, Namur, Belgium, 16–18 June, 2004.

60. Riccioli, C., Pérez-Marín, D., Guerrero-Ginel, J.E., Saeys, W., and Garrido-Varo, A. (2011) Pixel selection for near-infrared chemical imaging (NIR-CI) discrimination between fish and terrestrial animal species in animal protein by-product meals. *Appl. Spectros.*, 65: 771–781.

61. Kim, I., Kim, M.S., Chen, Y.R., and Kong, S.G. (2004) Detection of skin tumors on chicken carcasses using hyperspectral fluorescence imaging. *Agr. Eng.*, 47 (5): 1785–1792.

62. Lawrence, K.C., Windham, W.R., Park, B., and Buhr, R.J. (2003) An hyperspectral imaging system for identification of faecal and ingesta contamination on poultry carcasses. *J. Near Infrared Spectros.*, 11: 269–281.

63. Park, B., Lawrence, K.C., Windham, W.R., and Smith, D.P. (2005) Detection of cecal contaminants in visceral cavity of broiler carcasses using hyperspectral imaging. *Appl. Eng. Agr.*, 21: 627–635.

64. Wang, N. and El Masry, G. (2010) Bruise detection of apples using hyperspectral imaging. *Agr. Eng.*, 295–320.

65. Nagata, M., Tallada, J.G., Kobayashi, T., Cui, Y., and Gejima, Y. (2004) Predicting maturity quality parameters of strawberries using hyperspectral imaging. ASAE: St. Joseph, MI. ASAE/CSAE Paper No. 043033.

66. Nagata, M. and Tallada, J.G. (2008) Quality evaluation of strawberries. In *Computer Vision Technology for Food Quality Evaluation*, Sun, D.W., Ed. Academic Press: Amsterdam, pp. 265–287.

67. Cheng, X., Chen, Y.R., Tao, Y., Wang, C.Y., Kim, M.S., and Lefcourt, A.M. (2004) A novel integrated PCA and FLD method on hyperspectral image feature extraction for cucumber chilling damage inspection. *Society*, 47 (4): 1313–1320.

68. Lu, R. and Peng, Y. (2006) Hyperspectral scattering for assessing peach fruit firmness. *Biosyst. Eng.*, 93 (2): 161–171.

69. Wu, J., Peng, Y., Li, Y., Wang, W., Chen, J., and Dhakal, S. (2012) Prediction of beef quality attributes using VIS/NIR hyperspectral scattering imaging technique. *J. Food Eng.*, 109: 267–273.

70. Naganathan, G.K., Grimes, L.M., Subbiah, J., Calkins, C.R., Samal, A., and Meyer, G.E. (2008) Visible/near-infrared hyperspectral imaging for beef tenderness prediction. *Comput. Electron. Agr.*, 65 (2): 225–233.

71. Kim, C., Naganathan, G.K., Subbiah, J., Lu, R., Calkins, C.R., and Samal, A. (2008) Optical scattering in beef steak to predict tenderness using hyperspectral imaging in the VIS-NIR region. *Sensing and Instrumentation for Food Quality*, 2: 189–196.

72. Gómez-Sanchis, J., Moltó, E., Gomez-Chova, L., Aleixos, N., Camps-Valls, G., and Juste, F. (2008) Hyperspectral system for early detection of rottenness caused by *Penicillium digitatum* in mandarins. *J. Food Eng.*, 89 (1): 80–86.

73. Qin J., Burks, T.F., Ritenour, M.A., and Gordon Bonn, W. (2009) Detection of citrus canker using hyperspectral reflectance imaging with spectral information divergence. *J. Food Eng.*, 93: 183–191.

74. Fernández Pierna, J.A., Vermeulen, P., Amand, O., Tossens, A., Dardenne, P., and Baeten, V. (2012) NIR Hyperspectral imaging spectroscopy and chemometrics for the detection of undesirable substances in food and feed. *Chemometr. Intell. Lab. Syst*, 117: 233–239. doi: 10.1016/j.chemolab.2012.02.004

75. Abdel-Nour, N. and Ngadi, M. (2011) Detection of omega-3 fatty acid in designer eggs using hyperspectral imaging. *Int. J. Food Sci. Nutr.*, 62 (4): 418–422.

76. Peirs, A., Scheerlinck, N., Perez, A.B., Jancsok, P., and Nicolai, B.M. (2002) Uncertainty analysis and modelling of the starch index during apple fruit maturation. *Postharvest Biology and Technology*, 26 (2): 199–207.

77. Peirs, A., Scheerlinck, N., De Baerdemaeker, J., and Nicolai, B.M. (2003) Starch index determination of apple fruit by means of an hyperspectral near infrared reflectance imaging system. *J. Near Infrared Spectros.*, 11 (5): 379–389.

78. Menesatti, P., Zanella, A., D'Andrea, S., Costa, C., Paglia, G., and Pallottino, F. (2008) Supervised multivariate analysis of hyper-spectral NIR images to evaluate the starch index of apples. *Food Bioproc. Tech.*, 2 (3): 308–314.

79. Weinstock, A.B., Janni, J., Hagen, L., and Wright, S. (2006) Prediction of oil and oleic acid concentrations in individual corn (*Zea mays* L.) kernels using near-infrared reflectance hyperspectral imaging and multivariate analysis. *Appl. Spectros.*, 60 (1): 9–16.

80. Xing, J., Van Hung, P., Symons, S., Shahin, M., and Hatcher, D. (2009) Using a short wavelength infrared (SWIR) hyperspectral imaging system to predict alpha amylase activity in individual Canadian western wheat kernels. *Sensing and Instrumentation for Food Quality*, 3: 211–218.

81. Xing, J., Symons, S., Hatcher, D., and Shahin, M. (2011) Comparison of short-wavelength infrared (SWIR) hyperspectral imaging system with an FT-NIR spectrophotometer for predicting alpha-amylase activities in individual Canadian Western Red Spring (CWRS) wheat kernels. *Biosyst. Eng.*, 108: 303–310.

82. Burns, D.A. and Ciruczak, E.W. (2008) *Handbook of Near-Infrared Analysis,* 3rd ed. Taylor and Francis, Philadelphia.

83. Williams, P., Geladi, P., Fox, G., and Manley, M. (2009) Maize kernel hardness classification by near infrared (NIR) hyperspectral imaging and multivariate data analysis. *Anal. Chim. Acta*, 653: 121–130.

84. Bauriegel, E., Giebel, A., Geyer, M., Schmidt, U., and Herppich, W.B. (2011) Early detection of *Fusarium* infection in wheat using hyper-spectral imaging. *Comput. Electron. Agr.*, 75: 304–312.

85. Firrao, G., Torelli, E., Gobbi, E., Raranciuc, S., Bianchi, G., and Locci, R. (2010) Prediction of milled maize fumonisin contamination by multispectral image analysis. *J. Cereal Sci.*, 52: 327–330.

86. Del Fiore, A., Reverberi, M., Ricelli, A., Pinzari, F., Serranti, S., Fabbri, A.A., Bonifazi, G., and Fanelli, C. (2010) Early detection of toxigenic fungi on maize by hyperspectral imaging analysis. *Int. J. Food Microbiol.*, 144: 64–71.

87. Vermeulen, P., Fernández Pierna, J.A., Sinnaeve, G., Dardenne, P., and Baeten, V. (2009) Detection of ergot bodies in cereals by NIRS and hyperspectral NIR imaging. Poster session presented at the 14th ICNIRS, 7–13 November, Bangkok, Thailand.

88. Zijlstra, C., Lund, I., Justesen, A.F., Nicolaisen, M., Kryger Jensen, P., Bianciotto, V., Posta, K., Balestrini, R., Przetakiewicz, A., Czemborf, E., and van de Zande, J. (2011) Combining novel monitoring tools and precision application technologies for integrated high-tech crop protection in the future (a discussion document). *Pest Manag. Sci.*, 67: 616–625.

89. Vermeulen, P., Fernández Pierna, J., Tossens, A., Amand, O., Dardenne, P., and Baeten, V. (2011) Identification and quantification of cyst nematode in sugar beet seeds by hyperspectral NIR imaging. Paper read at the 14th ICNIRS, Bangkok, Thailand, 7–13 November, 2009, 997–1002.